

Cite this: *RSC Sustainability*, 2024, 2, 988Received 19th October 2023  
Accepted 30th January 2024

DOI: 10.1039/d3su00380a

rsc.li/rscsus

# Tailoring lignin nanoparticle properties: the effects of pH and salt on shape and antioxidant capacity†

Natalia Obrzut, Rob Hickmott and Kimberly Gray\*

In this study we explore the extent to which we can tune lignin nanoparticles produced in a biorefinery that couples a microbial electrolysis cell to lignin depolymerization. We vary the salt type and pH and monitor the size and shape of the nanoparticles, as well as the antioxidant capacity of the mixture. We found that the salt type influences the shape of the lignin nanoparticles – ranging from spherical (phosphate) to rod-like (nitrate and chloride) and flower-like (carbonate). Additionally, the shape and the size influence the antioxidant capacity due to changes in the surface area to volume ratio. The flower-like nanoparticles have a high surface area to volume ratio and the highest antioxidant capacity, which is similar to that of the industrial benchmark antioxidant, Trolox. The antioxidant capacity of the lignin nanoparticles illustrates their high potential value in the pharmaceutical, nutraceutical, personal care, and agricultural industries.

## Sustainability spotlight

Lignin is the only source of renewable aromatic carbon on the planet. However, its efficient conversion into valuable products is still being explored, specifically as a natural alternative source of antioxidants. This work aims to explore how the shape and antioxidant capacity of nanoparticles derived from lignin vary as a function of salt type and pH. The depolymerization performed in our biorefinery utilizes the high salt caustic effluent produced *via* a microbial electrolysis cell; therefore, it is important to understand how the salt and pH parameters can tune depolymerized products. Nanoparticles with high antioxidant capacity have high commercial value in various industries including in pharmaceuticals, nutraceuticals, and cosmetics. Our work emphasizes the importance of the following UN sustainable development goals: responsible consumption and production (SDG 12).

## Introduction

The Hofmeister series (Fig. 1), first reported over 100 years ago, systematically and empirically describes the specific ion effects of salts in relation to protein stability.<sup>4–7</sup> At one end of the scale, are the kosmotropic ions which are responsible for decreasing the solubility of proteins (*i.e.* salting out) and are often used to induce protein aggregation in pharmaceutical preparation at various stages of protein extraction and purification.<sup>6</sup> At the other end of the scale are the chaotropic ions, which denature and dissolve proteins (*i.e.* salting in). However, the Hofmeister series is not absolute. In fact, since the Hofmeister series is based on colloidal interactions with negatively charged hydrophobic surfaces, it may not apply to interactions with hydrophilic surfaces, at high salt concentrations, or at non-neutral pH.<sup>7</sup> Despite empirical knowledge about specific ion effects across various industries, a general predictive theory explaining these effects has yet to be developed. This is likely due to the complexity of interactions influenced by the properties of salts and colloidal surfaces, including ionic size, charge density and

distribution, polarizability, hydrophobicity and charge shielding, ion-pairing, solvation, permeability, complexation, stickiness, and interfacial disruption.<sup>5</sup>

We have previously reported work detailing a biorefinery that uses a cathodic effluent from a microbial electrolysis cell (MEC) to depolymerize lignin into phenolics, flavonoids, and lignin nanoparticles at ambient temperature and pressure.<sup>8</sup> Lignin depolymerized with the caustic (pH 10.8) and high salt (220 mM phosphate) MEC effluent was found to produce up to 50% phenolics, 20% flavonoids, and close mass balance with LNPs that were spherical, less than 500 nm in size, and stable.<sup>8</sup> Additionally, the product mixture had a high antioxidant capacity ( $IC_{50} = 34 \text{ mg L}^{-1}$ ).<sup>9</sup> Lignin nanoparticles are non-toxic, biodegradable, inexpensive, and stable. These characteristics make LNPs favorable alternatives to carbon-based nanoparticles for a variety of uses such as drug delivery, hydrogels, sunscreen, food additives, and tissue repair.<sup>10,11</sup> Figuring out

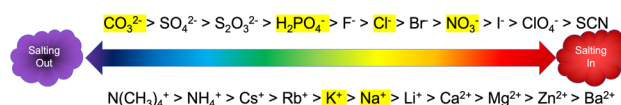


Fig. 1 The Hofmeister series adapted from Kang *et al.*<sup>4</sup> Anions are shown on the top of the scale and cations are shown on the bottom. The highlighted ions are the ones used in this study.

Department of Civil and Environmental Engineering, Northwestern University, 2145 Sheridan Road, Evanston, Illinois 60208, USA. E-mail: k-gray@northwestern.edu

† Electronic supplementary information (ESI) available. See DOI: <https://doi.org/10.1039/d3su00380a>



how to tune the shape and size of LNPs is an important step in increasing their commercial potential.

Following the success of these initial studies, we now aim to tune the size, shape, and antioxidant capacity of the lignin nanoparticles by modifying the salt type in accordance to the Hofmeister series, as well as varying the pH. Although the Hofmeister series has been primarily used to study the stability of proteins in solution, we hypothesize that the series may hold true for lignin as well. Lignin, like proteins, is a biopolymer with hydrophobic and hydrophilic regions and our biorefinery preserves these attributes in its depolymerization products. We hypothesize that it is possible to tune the products of lignin depolymerization to specifically favor the stabilization of lignin nanoparticles (LNPs) using kosmotropic salts (carbonate & phosphate) and favor the stabilization of phenolics and flavonoids with chaotropic salts (nitrate & chloride).

## Materials and methods

### Materials

Lignin was donated by Archer Daniels Midland (ADM), Decatur IL. ADM extracts lignin from corn stover by the acetosolv (organosolv using acetic acid) process. We used the following chemicals for depolymerization – sodium phosphate dibasic (Fischer), potassium phosphate monobasic (USP analytical test, JT Baker), sodium hydroxide (certified ACS, Fischer), phosphoric acid, sodium chloride (certified ACS, Fischer), sodium nitrate (certified ACS, Fischer), sodium carbonate (certified ACS, BDH), sodium bicarbonate (certified ACS, BDH). For flavonoid content we used: aluminum chloride hexahydrate (Alfa Aesar), sodium nitrite (98%, Alfa Aesar), methanol (HPLC grade, Fisher). For phenolic content we used: Folin–Ciocalteu reagent (Sigma Aldrich), sodium carbonate (ACS, VWR), gallic acid (97.5%, Sigma Aldrich). For antioxidant assay we used: rutin (>94%, TCI), Trolox (Abcam), ABTS (TCI), potassium persulfate (certified ACS, Fischer). Hexadecyltrimethylammonium bromide (CTAB) (>98%, Sigma Aldrich) was used in microscopy.

### Lignin solubilization

Lignin depolymerization was carried out as described in Obrzut *et al.*<sup>8</sup> Synthetic MEC catholyte (depolymerization media) was used for the experiments and prepared with different salts to a total molarity of 227 mM. Four different salts were used for the depolymerization media: sodium chloride (13 g L<sup>-1</sup>), sodium nitrate (19 g L<sup>-1</sup>), sodium carbonate/sodium bicarbonate (21 g per L Na<sub>2</sub>CO<sub>3</sub> and 2 g per L NaHCO<sub>3</sub>), and sodium phosphate dibasic/potassium phosphate monobasic (32 g per L Na<sub>2</sub>HPO<sub>4</sub> and 0.2 g per L KH<sub>2</sub>PO<sub>4</sub>·H<sub>2</sub>O). The four depolymerization media were adjusted to pH 10.8 for initial depolymerization. Chloride, nitrate, and phosphate were adjusted with sodium hydroxide to increase the pH, carbonate was adjusted with phosphoric acid to decrease the pH. The amounts of sodium hydroxide and phosphoric acid had negligible effect on the ionic strength.

Lignin depolymerization was conducted in a lab bench scale reactor (beaker) over 60 minutes. Lignin and depolymerization media were combined for a total concentration of 1 g L<sup>-1</sup>. Over

the course of 60 minutes the pH was monitored and adjusted to ±0.2 of pH 10.8 with sodium hydroxide, this amounted to 50–100 μL of sodium hydroxide for the chloride and nitrate based media. After the 60 minutes, basic experiments (b) were left as is, neutral samples (n) were neutralized with phosphoric acid to pH 7, and acidic samples (a) were acidified to pH 3.8.

The experiments were conducted at room temperature and observed for a total of one week at which point nearly all the lignin was in solution (Table S1 in the ESI†). Measurements for solubilization, phenolic content, flavonoid content, antioxidant capacity, LNP concentration, size, polydispersity index (PDI), and zeta potential were taken at day 0 and at day 7. The LNPs were observed under the SEM at day 7. Table S2 in the ESI† summarizes the type of salt used, concentration, pH and ionic strength.

### Measurement of bulk properties

The following properties were measured with UV-vis spectroscopy (Eppendorf BioSpectrometer): soluble lignin, total phenolic content, total flavonoid content, antioxidant capacity. These methods were previously described in Obrzut *et al.*<sup>8,9</sup> Total phenolic content and total flavonoid content were also measured after a series of filtrations for select experiments using PTFE filters with pore sizes 400 nm, 200 nm, and 100 nm.

Soluble lignin was determined through a calibration curve of lignin dissolved completely in pH 13 NaOH solution. The maximum absorbance occurred at 280 nm. Solubilization was measured on centrifuged samples to remove any residual solids or large LNPs that induce scattering in the spectroscopic readings. The total amount of phenolics was determined with the colorimetric Folin–Ciocalteu method.<sup>12</sup> The Folin–Ciocalteu method combines 100 μL of solubilized lignin with 2 mL of a 2% sodium carbonate solution. The mixture was incubated at room temperature for 5 minutes and then 100 μL of Folin–Ciocalteu reagent was added and the mixture was incubated further for 30 minutes. The absorbance was measured at 750 nm. A calibration was performed with a solution of gallic acid (3,4,5-trihydroxybenzoic acid) every time the experiment was performed.<sup>12</sup> The total amount of flavonoids was determined *via* the method by Zhishen *et al.*<sup>13</sup> For this method, 300 μL of solubilized lignin was combined with 3.4 mL of a 30% methanol solution, 150 μL of a 0.5 mmol per L sodium nitrate solution and 150 μL of a 0.3 mmol per L aluminum chloride hexahydrate solution at room temperature. 1 mL of 1 mol per L sodium hydroxide was added after 5 minutes and the absorbance was immediately measured at 510 nm. The calibration curve was made using the flavonoid rutin, (3',4',5,7-tetrahydroxy-3-[ $\alpha$ -L-rhamnopyranosyl-(1→6)- $\beta$ -D-glucopyranosyloxy]flavone). A 100 mg L<sup>-1</sup> sample of rutin was made with each set of experiments to test the accuracy of the calibration curve.

The antioxidant capacity was also determined by measuring absorbance. We followed a modified version of the ABTS method first described by Cano *et al.*<sup>14</sup> The ABTS<sup>+</sup> radical solution was prepared from 10 mL of 7 mM ABTS<sup>+</sup> [2,2'-azino-bis(3-ethyl-benzothiazoline-6-sulfonic acid)] solution in water and 10 mL of 2 mM potassium persulfate solution in water. The mixture was incubated in the dark at room temperature overnight. The ABTS<sup>+</sup> solution was diluted with water to an



absorbance of  $0.70 \pm 0.1$  at 734 nm. Then 1 mL of different concentrations of lignin (0, 2, 6, 10, 14, 16, 18, 20, 40, 60, 80, 100, 140, 160, 200, 300, 400, 600, 800  $\text{mg L}^{-1}$ ) were added to 2.0 mL of ABTS<sup>+</sup> diluted solution. The mixture was incubated in the dark for 6 minutes and were measured at 734 nm. The scavenging was calculated with the following equation:

$$\text{Scavenging effect (\%)} = \frac{A_c - A_t - CF}{A_c - CF} \times 100$$

where  $A_c$  is the absorbance of the ABTS<sup>+</sup> diluted solution without any antioxidants added,  $A_t$  is the absorbance of the test, and CF is the correction factor due to pH. The correction factor for neutral samples of all salts, and basic samples of nitrate and chloride based depolymerization media is 0, the correction factor for pH 10.8 for phosphate and carbonate based depolymerization media varies as a function of concentration, these values are shown in Table S3 in the ESI.† The concentration required to inhibit the ABTS<sup>+</sup> by 50% ( $\text{IC}_{50}$ ) was determined by linear regression analysis. Trolox (6-hydroxy-2,5,7,8-tetramethylchroman-2-carboxylic acid) was used as a standard to verify the method. The  $\text{IC}_{50}$  of Trolox was found to be 21.5  $\text{mg L}^{-1}$ , consistent with literature reports.<sup>15</sup>

### Measurement of nanoparticles

LNP concentration, size, PDI, and zeta potential were determined with Nanoparticle Tracking Analysis (NTA) and Zetasizer. The NTA (Malvern Panalytical NanoSight NS300) was used according to Obrzut *et al.* to estimate both the LNP concentration and size distribution.<sup>8</sup> The concentration of LNPs according to this method is reported in Table S1 in the ESI.† The lignin solutions were diluted 50 times in water to be measured *via* NTA. The Zetasizer (Malvern Panalytical Zetasizer Nano ZS) also has dynamic light scattering (DLS) capabilities to measure size and polydispersity index. The lignin solutions were diluted 10× for size and PDI and 50× for zeta potential measurements. Then, 1 mL of sample was placed in a DTS1070 disposable zeta potential cuvette or a plastic cuvette for DLS. Three measurements were taken for each sample with up to 100 zeta runs per sample. For these runs the refractive index of lignin was set at 1.61.<sup>16</sup>

The SEM micrographs were obtained using a JEOL JSM-7900FLV microscope equipped with an Oxford Ultimex 65 energy-dispersive X-ray spectroscopy (EDS) accessory. The voltage was set to 5 kV and the current to 8 mA. The SEM was run using the lower electron detector (LED). The software AZtecLive was used for live elemental mapping. SEM samples were prepared by diluting the suspensions 10-fold with a surfactant (5% CTAB solution) and sonicating them.

## Results and discussion

### The effect of salt type on shape

The biggest impact of salt type on LNP formation is revealed in the SEM images illustrated in Fig. 2 showing three different LNP shapes (flower-like, spheres, and rods). The simple salt mixtures ( $\text{NO}_3^-$  &  $\text{Cl}^-$ ) generate small spheres under basic conditions (Fig. 2e–g) that become larger and rod-shaped at pH

7 (Fig. 2f–h). LNP mixtures in phosphate buffer at both pHs but higher ionic strength than the simple salt mixtures, are large spheres (Fig. 2c and d). In a carbonate buffered mixture (basic pH,  $I \approx 0.5$  M), LNPs form a distinct, flower-like structure large in size (Fig. 2a), which collapse to oblong spheres at pH 7 and  $I \approx 0.2$  M (Fig. 2b). For a particular salt type, the shape of the LNP typically depends on pH, except in the case of phosphate, where both in neutral and basic conditions spherical LNPs are observed (Fig. 2c and d).

In Table 1, possible hydrophilic (blue)/hydrophobic (orange) LNP structures are proposed to explain the shapes observed in the SEM images. Briefly, a spherical micelle is typically formed when the polymer has a long hydrophilic head and a short hydrophobic tail, the opposite is true for rod-like micelles (short hydrophilic head and long hydrophilic tail). Flower-like micelles are characterized by three sections, a long hydrophilic head and two short hydrophobic tails. Table 2 presents the EDS data of the LNPs and shows that spherical and flower-like micelles have a greater oxygen content than the rod-like micelles, indicating that the hydrophilic heads may, in fact, be longer. We also show that the salts do not react with the LNPs as they are not present in the EDS data of the LNPs (EDS spectra are shown in Fig. S1 in the ESI†). Furthermore, an additional experiment was conducted by dialyzing the LNPs to remove the salt and an SEM image of the resulting flower-like LNP can be found in Fig. S2 in the ESI.† LNP shape, then, is determined by a complex set of interactions between size/structure of soluble lignin oligomeric subunits, specific chemical interactions between salt ions and lignin subunits, attractive/repulsive electrostatic interactions, hydrophobic/hydrophilic interactions, pH, ionic strength, *etc.*

The different LNP shapes shown in Fig. 2 may have an influence on the antioxidant capacity due to differences in the surface area to volume ratio ( $\text{SA} : V$ ). Fig. 3 compares the antioxidant capacity corresponding to LNPs in Fig. 2a, c, f and h, and shows that the flower-like micelle (carbonate) has the highest antioxidant capacity (lowest  $\text{IC}_{50}$ ), likely due to the fact that it has the higher surface area. Hydrophilic phenolic groups on the external surface of the LNP micelle are responsible for the free radical scavenging. Hence, the greater the LNP surface area, the greater the amount of exposed phenolic groups and

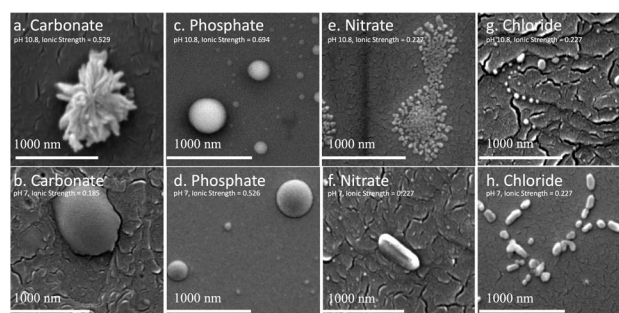

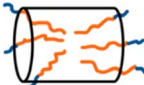



Fig. 2 SEM images of select LNPs, all taken at  $t = 7$  d. (a) carbonate, basic,  $I = 0.529$ ; (b) carbonate, neutral,  $I = 0.185$ ; (c) phosphate, basic,  $I = 0.694$ ; (d) phosphate, neutral,  $I = 0.526$ ; (e) nitrate, basic,  $I = 0.227$ ; (f) nitrate, neutral,  $I = 0.227$ ; (g) chloride, basic,  $I = 0.227$ ; (h) chloride, neutral,  $I = 0.227$ .



**Table 1** The different micelle shapes assumed by lignin LNPs.<sup>1,2</sup> Orange indicates the hydrophobic tail and blue indicated the hydrophilic head

| Diagram   | Shape       | Description  |
|---|-------------|--|
|  | Spherical   | Long hydrophilic head, short hydrophobic tail            |
|  | Rod-like    | Short hydrophilic head, long hydrophobic tail            |
|  | Flower-like | Long hydrophilic section, two short hydrophobic sections |

the greater the antioxidant capacity.<sup>9,17,18</sup> It is worth noting that the antioxidant capacity of the carbonate based LNP is consistent with the antioxidant capacity of the industrial standard, Trolox. The spherical LNPs formed by phosphate salts have the second highest antioxidant capacity. From the SEM image in Fig. 2c, we observe three differently sized spherical LNPs at a radius of around 300, 160, and 40 nm, corresponding to an average surface area to volume ratio of around 0.4. The rod-like LNPs have the lowest SA:V ratio and the lowest antioxidant capacity. In Fig. 2f, we observe a rod-like LNP with a radius corresponding to 110 nm, and a length of 550 nm, which gives a SA:V ratio of 0.2 nm, half the SA:V of the mixture of spherical LNPs. Shape is not the only factor that controls the SA:V ratio, the size (*i.e.* the radius) also has an effect. Typically, the smaller the radius, the larger the SA:V ratio, and specifically, we observe that under basic conditions the LNPs are smaller and tend to show greater the antioxidant capacity. We may also note here that the antioxidant capacity is measured on the entire depolymerized lignin mixture, which includes both LNPs and discrete phenolics/flavonoids, which have different antioxidant properties. Further discussion on these differences follow in the next section.

### pH and the Hofmeister effect on the stability of products

As mentioned in the introduction, the Hofmeister series is an empirical series that is used to explain the stability of proteins due to salt effects. In this paper we aimed to test whether we can apply the Hofmeister series to tune LNP properties. Fig. 1 in the introduction shows the Hofmeister series, highlighting the anions and cations we chose to use for our experiments. When the Hofmeister series is used in reference to proteins, salting out indicates that the proteins are stabilized and their folding is intact. Salting in indicates that proteins are denatured and unfolded (Fig. 4a). In regard to depolymerized lignin stabilization, salting out would promote the self-assembly of depolymerized lignin oligomers in the form of LNPs, whereas salting in would favor depolymerized lignin as discrete phenolics and flavonoids and hinder LNP formation (Fig. 4b). Although we should not expect strict adherence to the Hofmeister series, we do see similar trends between salts at opposite ends of the scale.

We typically conduct all our measurements, except solubilization, on uncentrifuged samples.<sup>8,9</sup> Our aim is to characterize the mixture as a whole and demonstrate its potential in industrial applications without separation or purification. Given differences in LNP characteristics and antioxidant

**Table 2** EDS for select LNP samples. All values are in percentages (%). All samples indicate that the LNPs are made almost exclusively ( $\geq 90\%$ ) of carbon and oxygen. Carbon is denoted in orange to correspond to the orange, hydrophobic block in Table 1 and oxygen is denoted in blue to correspond to the blue, hydrophilic block in Table 1

| Element/Anion-pH    | C     | O     | N | Cl    | P    | Na   | K    | Br   |
|---------------------|-------|-------|---|-------|------|------|------|------|
| Cl - n              | 82.72 | 6.44  | 0 | 1.92  | 0    | 4.23 | 0    | 4.68 |
| NO <sub>3</sub> - n | 86.72 | 10.90 | 0 | 0     | 0    | 2.39 | 0    | 0    |
| CO <sub>3</sub> - b | 77.68 | 16.40 | 0 | 0.012 | 0    | 0.52 | 0.02 | 5.25 |
| PO <sub>4</sub> - n | 77.54 | 16.23 | 0 | 0.19  | 1.11 | 0.19 | 0    | 4.74 |



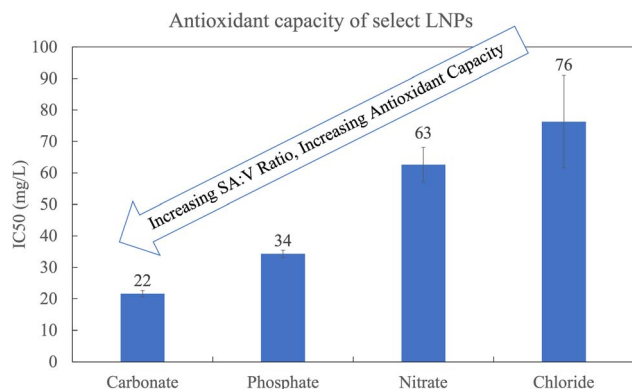


Fig. 3 The antioxidant capacity corresponding to the LNPs in Fig. 2a, c, f and h. All at  $t = 7$  days.  $\text{CO}_3$  and  $\text{PO}_4$  are at pH 10.8 and  $I = 0.529$  and  $I = 0.694$ , respectively.  $\text{NO}_3$  and Cl are at pH 7.0 and  $I = 0.227$ .



Fig. 4 (a) The Hofmeister series effect on protein stabilization. (b) The hypothesized stability of depolymerized lignin with respect to ion type is illustrated.

capacity among conditions, however, it is likely that some fraction of bulk phenolic and flavonoid content is associated with the colloidal fraction of lignin depolymerization mixtures.

Here, we characterize product yields and properties in the lignin depolymerization mixtures of various salts as a function of colloidal size based on differential filtration and compare centrifugation to filtration through 400 nm, 200 nm, 100 nm pore size membranes. These data are shown in Fig. 5 for the two salts, carbonate and nitrate, at the extremes of the Hofmeister series.

The filtration results presented in Fig. 5 illustrate that the phenolic and flavonoid fraction display a greater degree of association with the colloidal or LNP fraction under neutral conditions ( $p > 0.05$ ) compared to basic pH. In previous work, we showed that the predominant flavonoid present in depolymerized organosolv lignin from corn stover in our biorefinery is tricetin, at 2.8%.<sup>8</sup> The  $pK_a$  of tricetin is 6.57, indicating that at a basic pH, the pH is much greater than the  $pK_a$ , and the tricetin and other phenolic groups are deprotonated. Therefore, phenolics and flavonoids are stabilized by electrostatic interactions at basic pH and do not associate with other flavonoids and LNPs. At neutral conditions, however, the pH is about the same as the  $pK_a$  and not all of the phenolic groups are deprotonated. This suggests less electrostatic repulsion, and flavonoids and phenolic may be associated with the LNPs. When the flavonoids and phenolics associate or partition with the LNPs, we are able to filter them out, which then explains the decrease in phenolic and flavonoids at neutral pH but not in basic conditions.

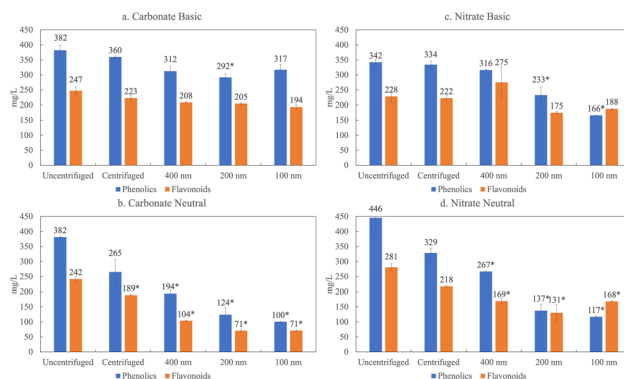


Fig. 5 The phenolic (blue) and flavonoid (orange) content for carbonate based lignin depolymerization in (a) basic and (b) neutral conditions and nitrate based lignin depolymerization (c) basic and (d) neutral conditions across different filtrations. \*Indicates a significant difference ( $p < 0.05$ ) relative to the uncentrifuged sample.

The filtration results in Fig. 5 also reveal a salt effect. When we compare the amount of phenolics and flavonoids present in lignin depolymerized with carbonate at 100 nm, we witness a 60% decrease in phenolics and 70% decrease in phenolics at neutral pH. In contrast, with nitrate based depolymerization only an 11% decrease for flavonoids and 31% decrease for phenolics occur. This trend is consistent with the Hofmeister series. Carbonate, which is on the far left side of the series, favors salting out, which in this case would favor the stabilization of LNPs and partitioning of phenolics and flavonoids in the colloidal fractions. Nitrate is on the far right side, which would indicate salting in, suggesting more favorable conditions to stabilize phenolics/flavonoids. This observation is summarized in Fig. 4b which illustrates the correspondence of the Hofmeister series to depolymerized lignin products.

### The effect of pH on the mechanism of LNP formation

It is well known that there are generally two accepted mechanisms of formation for lignin nanoparticles – acid precipitation and solvent/antisolvent. We show a schematic of both in Fig. 6.

Generally, the formation of LNPs relies first on dissolving lignin.<sup>19–26</sup> The lignin can generally be dissolved in two ways: (1) high pH or (2) an organic solvent. High pH is not a very common way of dissolving lignin for LNP production, and most researchers opt for organic solvents. For acid precipitation, the second step is to then decrease the solubility of lignin with the addition of an acid. LNP formation is initiated by the molecular weight dependent precipitation of the dissolved subunits of lignin, where large molecules precipitate first to form a critical nuclei (40–70 nm).<sup>27</sup> This is followed by collision-driven particle growth and adsorption.

The solvent/antisolvent mechanism is initiated in the same way, the first step is to dissolve the lignin with an organic solvent such as DMSO or acetone. Then micellization is induced through the addition of an antisolvent, typically water. Micellization involves alignment of the hydrophobic and hydrophilic parts of the lignin depending on the solvent characteristics.<sup>28</sup> Lignin subunits aggregate in the water phase to form



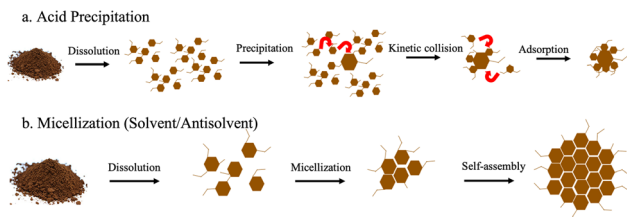


Fig. 6 (a) Acid precipitation and (b) micellization mechanisms of formation for lignin nanoparticles adapted from Obrzut and Gray.<sup>5</sup>

a hydrophobic micellar core. The hydrophilic components of the lignin form the micelle shell. The LNPs grow spherically through either molecular aggregation of polymer chains or by self-assembly *via* aromatic stacking.<sup>24,29</sup>

Although our method of lignin depolymerization and LNP formation involves a basic depolymerization media, not an organic solvent, and the pH is sometimes adjusted to neutral, the mechanism of formation has been shown to be micellization.<sup>8</sup> We further demonstrated that this is indeed the mechanism by doing an additional experiment of adjusting the pH of depolymerized lignin to pH 3.8. We show the SEM image of phosphate depolymerized lignin at three different pH values in Fig. 7.

In Fig. 7a and b the shape of the LNPs is spherical and they are on average between 400 and 500 nm. The shape of the LNP formed in acidic conditions is amorphous and much larger ( $\sim 6\times$ ). The mechanism of formation most likely switches from micellization to acid precipitation, as seen by the drastic change in shape and size. We also see that the antioxidant capacity decreases. The  $IC_{50}$  increases from  $30\text{ mg L}^{-1}$  to  $390\text{ mg L}^{-1}$  with the change from basic to acidic LNPs. This indicates that for most commercial purposes LNPs formed in basic to neutral conditions are more favorable due to their spherical shape, small size, and high antioxidant capacity. It may be worth noting that LNP formation and growth in basic and neutral conditions is gradual (7 days to reach max concentration under our experimental condition, ambient  $T$  &  $P$ ), but maximum concentration is achieved instantly in acidic conditions.

One additional observation is that ionic strength effects were probed by modifying the concentration of the salt and found not to be a driving force in determining differences in LNP properties. These results are presented in Fig. S3 in the ESI.† This further supports the finding that LNP properties can be tuned by salt type and pH.

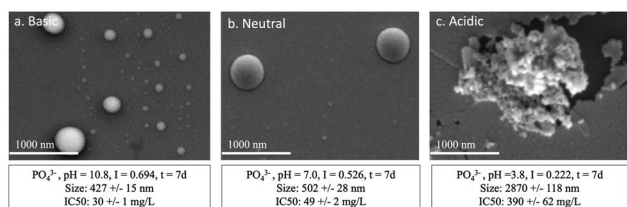


Fig. 7 The SEM image of LNPs formed through phosphate based depolymerization (220 mM, initial pH 10.8). The pH after 1 hour was (a) unadjusted, (b) neutralized, and (c) acidified. The size and antioxidant capacity is also reported.

## Conclusions

The goal of this research was to determine whether LNPs can be tuned in accordance with the Hofmeister series and pH adjustment. We found that the use of different salts (kosmotropic *versus* chaotropic) in the depolymerization of lignin allows us to tune the shape and antioxidant capacity of the resulting LNPs. Furthermore, we found that carbonate-based depolymerization yields flower-like LNPs that have an antioxidant capacity comparable to that of Trolox, a water-soluble analog of vitamin E used industrially in biological and biomedical applications. Phosphate-based LNPs are spherical, with a slightly lower antioxidant capacity. Nitrate- and chloride-based depolymerization produces rod-like LNPs with an antioxidant capacity 2–3 times lower than that of carbonate and phosphate. These results indicate that high antioxidant LNPs are promoted by the use of a carbonate buffered, caustic catholyte for lignin depolymerization in a MEC-based biorefinery.

We also found that the salts stabilize LNPs or phenolics/flavonoids in accordance with the Hofmeister series. Carbonate-based depolymerization favors the association of phenolics and flavonoids to LNPs with neutralization, whereas nitrate favors the stabilization of phenolics/flavonoids in solution.

The mechanism of LNP formation and therefore their characteristics are influenced by pH. In a phosphate buffer at neutral and basic pH, small and spherical LNPs form through micellization. At basic pH the LNPs are around 430 nm with an  $IC_{50}$  of  $30\text{ mg L}^{-1}$  and the neutral LNPs are slightly larger at around 500 nm with a slightly higher  $IC_{50}$  ( $50\text{ g L}^{-1}$ ), indicating a lower antioxidant capacity than the basic LNPs. LNPs formed in acidic conditions are formed *via* the acid precipitation mechanism and differ significantly in shape, size, and antioxidant capacity (amorphous, 2900 nm,  $390\text{ mg L}^{-1}$ , respectively).

This study allows us to better understand how salt and pH can be used to tune the properties of LNPs and expand potential industrial uses, particularly for nutraceutical applications where there is a recent rejection of synthetic antioxidants.<sup>30</sup> Although the synthesis time is lengthy, we see a high conversion of lignin into LNPs (Table S1†). Preliminary experiments demonstrate that our biorefinery produces proportional amounts of LNPs when doubled, indicating a potential for scaling. It is valuable to conduct future work investigating the limits of scalability to determine the conditions of commercialization.

## Conflicts of interest

There are no conflicts to declare.

## Acknowledgements

Funding for this work was provided by the Finite Earth Initiative of the McCormick School of Engineering at Northwestern University. Biological and chemical analysis was performed in the Analytical bioNanoTechnology Core Facility of the Simpson Querrey Institute at Northwestern University. The U.S. Army



Research Office, the U.S. Army Medical Research and Materiel Command, and Northwestern University provided funding to develop this facility and ongoing support is being received from the Soft and Hybrid Nanotechnology Experimental (SHyNE) Resource (NSF ECCS-1542205). This work made use of the IMSERC MS facility at Northwestern University, which has received support from the Soft and Hybrid Nanotechnology Experimental (SHyNE) Resource (NSF ECCS-2025633), and Northwestern University. This work also made use of the EPIC facility of Northwestern University's NUANCE Center, which has received support from the SHyNE Resource (NSF ECCS-2025633), the IIN, and Northwestern's MRSEC program (NSF DMR-1720139).

## References

- G. Gaucher, *et al.*, Block copolymer micelles: preparation, characterization and application in drug delivery, *J. Controlled Release*, 2005, **109**(1–3), 169–188.
- N. Hameed, *et al.*, Flower like micellar assemblies in poly(styrene)-block-poly(4-vinyl pyridine)/poly(acrylic acid) complexes, *Mater. Lett.*, 2015, **147**, 92–96.
- N. Obrzut and K. Gray, Chapter 17: Biorefining renewable aromatic carbon: unlocking lignin's potential to produce high-value products, in *Photosynthesis*, ed. H. Hou, Elsevier, 2023.
- B. Kang, *et al.*, Hofmeister Series: Insights of Ion Specificity from Amphiphilic Assembly and Interface Property, *ACS Omega*, 2020, **5**(12), 6229–6239.
- K. P. Gregory, *et al.*, Understanding specific ion effects and the Hofmeister Series, *Phys. Chem. Chem. Phys.*, 2022, **24**(21), 12682–12718.
- A. M. Hyde, *et al.*, General Principles and Strategies for Salting-Out Informed by the Hofmeister Series, *Org. Process Res. Dev.*, 2017, **21**(9), 1355–1370.
- N. Schwierz, *et al.*, Reversed Hofmeister Series—The rule rather than the exception, *Curr. Opin. Colloid Interface Sci.*, 2016, **23**, 10–18.
- N. Obrzut, *et al.*, Valorization of Lignin under Mild Conditions: Biorefining Flavonoids and Lignin Nanoparticles, *ACS Sustain. Chem. Eng.*, 2022, **11**(2), 491–501.
- N. Obrzut, *et al.*, The effects of lignin source and extraction on the composition and properties of biorefined depolymerization products, *RSC Sustainability*, 2023, **1**, 2328–2340.
- A. Henn and M. L. Mattinen, Chemo-enzymatically prepared lignin nanoparticles for value-added applications, *World J. Microbiol. Biotechnol.*, 2019, **35**(8), 125.
- S. Iravani and R. S. Varma, Greener synthesis of lignin nanoparticles and their applications, *Green Chem.*, 2020, **22**(3), 612–636.
- A. Khorasani Esmaili, *et al.*, Antioxidant Activity and Total Phenolic and Flavonoid Content of Various Solvent Extracts from *In Vivo* and *In Vitro* Grown *Trifolium pratense* L. (Red Clover), *BioMed Res. Int.*, 2015, **2015**, 1–11.
- J. Zhishen, T. Mengcheng and W. Jianming, The determination of flavonoid contents in mulberry and their scavenging effects on superoxide radicals, *Food Chem.*, 1999, **64**(4), 555–559.
- A. Cano, M. Acosta and M. B. Arnao, A method to measure antioxidant activity in organic media: application to lipophilic vitamins, *Redox Rep.*, 2000, **5**(6), 365–370.
- H. Noreen, *et al.*, Measurement of total phenolic content and antioxidant activity of aerial parts of medicinal plant *Coronopus didymus*, *Asian Pac. J. Trop. Med.*, 2017, **10**(8), 792–801.
- Y. Li, *et al.*, Optically Transparent Wood from a Nanoporous Cellulosic Template: Combining Functional and Structural Performance, *Biomacromolecules*, 2016, **17**(4), 1358–1364.
- I. V. Pylypchuk, *et al.*, New Insight into the Surface Structure of Lignin Nanoparticles Revealed by 1H Liquid-State NMR Spectroscopy, *ACS Sustain. Chem. Eng.*, 2020, **8**(36), 13805–13812.
- L. Yao, *et al.*, Correlations of the physicochemical properties of organosolv lignins from *Broussonetia papyrifera* with their antioxidant activities, *Sustainable Energy Fuels*, 2020, **4**(10), 5114–5119.
- C. Frangville, *et al.*, Fabrication of environmentally biodegradable lignin nanoparticles, *Chemphyschem*, 2012, **13**(18), 4235–4243.
- M. Lievonon, *et al.*, A simple process for lignin nanoparticle preparation, *Green Chem.*, 2016, **18**(5), 1416–1422.
- Y. Qian, *et al.*, Fabrication of uniform lignin colloidal spheres for developing natural broad-spectrum sunscreens with high sun protection factor, *Ind. Crops Prod.*, 2017, **101**, 54–60.
- O. u. Rahman, *et al.*, Lignin nanoparticles: synthesis, characterization and corrosion protection performance, *New J. Chem.*, 2018, **42**(5), 3415–3425.
- A. P. Richter, *et al.*, Synthesis and Characterization of Biodegradable Lignin Nanoparticles with Tunable Surface Properties, *Langmuir*, 2016, **32**(25), 6468–6477.
- M. Si, *et al.*, Synchronous and rapid preparation of lignin nanoparticles and carbon quantum dots from natural lignocellulose, *Green Chem.*, 2018, **20**(15), 3414–3419.
- D. Tian, *et al.*, Lignin valorization: lignin nanoparticles as high-value bio-additive for multifunctional nanocomposites, *Biotechnol. Biofuels*, 2017, **10**, 192.
- J. Wang, *et al.*, Atomic Force Microscopy and Molecular Dynamics Simulations for Study of Lignin Solution Self-Assembly Mechanisms in Organic-Aqueous Solvent Mixtures, *ChemSusChem*, 2020, **13**(17), 4420–4427.
- M. H. Sipponen, *et al.*, Understanding Lignin Aggregation Processes. A Case Study: Budesonide Entrapment and Stimuli Controlled Release from Lignin Nanoparticles, *ACS Sustain. Chem. Eng.*, 2018, **6**(7), 9342–9351.
- Y. Qian, *et al.*, Formation of uniform colloidal spheres from lignin, a renewable resource recovered from pulping spent liquor, *Green Chem.*, 2014, **16**(4), 2156–2163.
- P. K. Mishra and A. Ekielski, The Self-Assembly of Lignin and Its Application in Nanoparticle Synthesis: A Short Review, *Nanomaterials*, 2019, **9**(2), 243.
- F. Shahidi and Y. Zhong, Measurement of antioxidant activity, *J. Funct. Foods*, 2015, **18**, 757–781.

